10.1071/PVv2016n182p43

InSAR: an introduction

Duan Uys
Department of Earth and Planetary Sciences
Macquarie University
duan-hugo.uys@students.mq.edu.au

Synthetic aperture radar (SAR) is a mature technology that has given birth to Interferometry SAR (InSAR). Comparing phase differences between two or more SAR images separated either by time or space makes it is possible to look at the world in three-dimensions. InSAR has many practical and academic applications ranging from measuring surface deformation to monitoring geomorphic processes. Using InSAR, for example, scientists have been able to precisely measure the after-effects of earthquakes, and to map glacial flow and ocean currents. In the industrial sector InSAR has been already been applied to the monitoring of mine sites and landslides – and has potential value in any area wherever natural displacement hazards exist.

InSAR data can be processed using commercial or open-source programs. GMTSAR, ROI PAC, and NEST-Snap are among the more powerful open-source packages that are readily available to the public. In most circles InSAR is still considered a new technology but it shows considerable promise as a powerful tool for mapping and monitoring earth surface processes; servicing both academic and industry interests.

History of development

In all sciences, there is an elegant dance between engineering and discovery. SAR (Synthetic Aperture Radar) was invented for a purpose. In the 1940s it was a military reconnaissance tool. In the 1950s it answered the need for an all-weather, 24-hour aerial remote surveillance device (Engineering and Technology History, 2015). Radar had been a popular method for obtaining aerial images of the ground because it was not weather or time dependent; relying on the electromagnetic radiation wavelength of microwave and radio proportions. However, because of physical limitations, radar antennas needed to be the size of a football field to obtain a suitable resolution for practical purposes. This caused a problem for many organisations needing high quality imagery. SAR methods use normal aperture radars across spatial distance to emulate a large radar antenna. Carl Wiley of Goodyear Aircraft Company (known later as Lockheed Martin) achieved fame as the father and inventor of SAR methods (Lasswell, 2005). Over the decades since it was first invented SAR has become the most used technique for obtaining radar imagery, servicing countless organisations stretching over many diverse sectors.

SAR gave birth to InSAR (Interferometry SAR). InSAR uses repeat-pass techniques to obtain two SAR images of a region over different times. An interferometry diagram is created to compare the phase differences (UNSW, 2004). The InSAR concept was developed not long after the invention of SAR. However, the computer power required to process InSAR data was not readily available back in the 1950-60s. InSAR data processing did not become practical until the early 1990s (GSI, 2004).

SEASAT, the first satellite platform with a SAR sensor on board, was launched in 1978 (Ferretti, 2013). RADARSAT-1, a well-known and popular satellite, was launched in 1995 (Canadian Space Agency, 2014) and operated at 5.3GHz, in the C-band wavelength (Canadian Space Agency, 2015). Over the next few years, more satellites equipped with the instruments for InSAR methods were launched and the data became more readily available. The combination of data availability and computer power allowed InSAR methods to develop.

Theory

An understanding of SAR is a necessary precursor to an understanding of InSAR. In conventional methods the purpose of SAR imagery is to measure the distance to a target of interest (Hensley and Rosen, 2001). The drawback to traditional SAR is that it views a three-dimensional world in planimetric view as shown in Figure 1. The main platforms used for SAR imagery are mounted on satellites and space shuttles and, because of their orbital paths around the Earth, the information recorded in a SAR image is plotted on a two-dimensional graph with the range, cross-track, as one axis and the azimuth, along-track, as

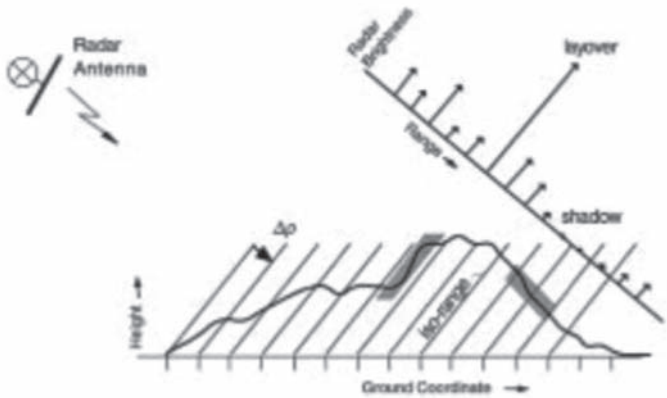

Figure 1. *Conventional SAR image forces a 3-D terrain to collapse into a 2-D profile. The brightness recorded indicates the amplitude of the return signal. The profile above is spatially distributed according to the distance to the radar defined by: Δρ=c/2Δf_BW – where c is the speed of light and Δf_BW is the range bandwidth of the radar. Figure from Hensley and Rosen, 2001.*

the other. As SAR operates mostly in a two-dimensional environment, plane and amplitude variations limit interpretation. InSAR adds a third dimension (either time or space). Currently InSAR is mostly applied to (1) topographic mapping and (2) surface deformation monitoring (Hensley and Rosen, 2001). This review will focus on the latter application, which has the potential to be particularly advantageous in industry sectors.

InSAR works around the concept of using phase delay information for each radar pulse pixel. When an EM (Electromagnetic) wave transmits from a radar, the corresponding backscatter return signal always has an associated phase delay given by the signal as a function of time:

$$S_r(t) = Acos[2\pi f_o(t-\tau)] \ (1.1)$$

Where $\tau = 2x/c$; the time it takes for the signal to travel to target and back; pulse delay; c is the speed of an electromagnetic wave in the appropriate medium. EM waves, being thought of transitional waves, display a sinusoidal form, and using $\lambda = \frac{c}{f_o}$ we can rearrange equation 1.1:

$$S(t) = Acos[2\pi f_o t - \phi] \ (1.2)$$

Where $\phi = -\frac{4\pi}{\lambda}x$; known as the phase delay. This is the fundamental concept that gives InSAR its power. The phase delay may include a noise contribution, but for simplicity it is usually ignored (Ulaby and Long, 2014). InSAR methods are based on combining radar return signals from two different SAR images separated in space (topography) or time (surface deformation). When monitoring surface deformation the phase delay is compared between two SAR images at different times.

Modulo-2π

The concept of Modulo-2π is important to grasp, because it allows us to understand something, but not everything, about what is going on (Ferretti, 2013). Because of EM wave properties, the sensor-to-target is better expressed as a number of wavelengths, plus a segment equal to a fraction of λ. To better clarify this thought, suppose a radar antenna is operating in the X-band with a wavelength of about 3 cm. The point of interest is 30 m away. In this case, the sensor-target distance is exactly 1000 wavelengths, $1000\lambda = \frac{30m}{0.03m}$. Considering a two-way path for the signal, the total distance would be equal to 2000 wavelengths. Now consider moving the same target 0.50 cm towards the radar, corresponding to surface inflation, the signal would not have to travel as far. In fact, it would take only 999 wavelengths plus 0.83λ, corresponding to a total 1999 full wavelengths plus 0.66λ for two-way travel. We needed one-third less of a wavelength to complete the sensor-target distance the second time around. As a consequence, in this example, the return signal for the second run would correspond to a phase value of $\phi = -\frac{\pi}{3}$.

Although this method is very effective at measuring deformation, if inflation or deflation equals half of a wavelength this wouldn't correspond to any phase shift. This is because moving the point 1.5 cm away/toward the distance travelled by the radar pulse would equal $2 \times 30.015 = 60m + 3cm$, and this would correspond to a full complete wavelength (Ferretti, 2013). Also known as the *effective wavelength* - $\lambda/_2$, any shift that coincides with multiples of the effective wavelength will not result in a phase change. Without prior information all that would be known is that a phase shift has occurred of $\phi = \pi$, but it would not be certain whether the shift is towards or away from the sensor. A good analogy would be waking in a dark room with a clock on the wall. The clock indicates that is 12 o' clock, but without prior knowledge and other information it wouldn't be clear whether it is midday or midnight.

Surface deformation

Studies of surface deformation using InSAR are more complex than studies of topography. Surface deformation studies also include motion, such as the movements of glaciers, ocean currents, and sand dunes. These studies can be an important investment in certain industries where valuable property could be affected by geomorphic processes. Surface deformation is calculated using along-track interferometry. This is because by altering the imaging geometry to an along-track path InSAR measures surface motion rather than topography (Ulaby and Long, 2014). To create time separated InSAR images an equation must to be derived to account for the complexity of satellite systems. Originally, before satellites became a major source of InSAR data, aeroplanes were used. Two SAR sensors would be mounted on the side of an aeroplane, one at the nose and the other at the tail as shown in Figure 2. This allowed two SAR images to be taken in the same spatial area, but at different times. If no cross-track displacement has occurred any return response due to topographic signal would, in theory, be null. A response, therefore, must be due to surface deformation/motion.

Figure 3 shows an example situation whereby an object of interest recedes from the aeroplane mounted with SAR sensors. At t_1, A_1 captures a SAR image with a distance to target of R_1. After a time, $t = {}^{B}/_{u}$, sensor A_2 is in the same position as the former sensor with a distance shown by:

$$R_2 = R_1 \pm \frac{B}{u} v_r \, sin\theta \ (1.3)$$

Where v_r is the radial velocity that corresponds to the velocity that the object of interest recedes or advances relative to the sensor position; θ coincides with the incidence angle. Putting this into terms of interferometric phase this conforms too:

$$\Delta\phi = \phi_1 - \phi_2 = -\frac{4\pi}{\lambda}(R_1 - R_2) \ (1.4)$$

$$\Delta\phi = \pm\frac{4\pi}{\lambda u} B v_r sin\theta \ (1.5)$$

By studying this equation, the interferometric phase is directly proportional to the radial velocity (Ulaby and Long, 2014). Equation 1.5 can be rearranged to solve for radial velocity:

$$\pm v_r = \frac{\lambda u}{4\pi B \, sin\theta} \phi_{int} \ (1.6)$$

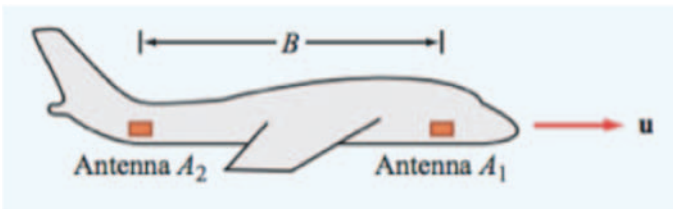

Figure 2. *Time separated SAR setup on an aeroplane. With a linear velocity of u and coupled with a baseline of B. A SAR image would be taken from A_1 after a time t=B/u has passed another SAR image would be taken at A_2. This would allow two different SAR images taken in same spatial area at different times. If topographic responses are assumed to be null (no cross-track displacement has occurred), any responses must be due to surface deformation/motion. Assuming backscatter amplitudes at both times are the same, ϕ_s1=ϕ_s2. Figure from Ulaby and Long, 2014.*

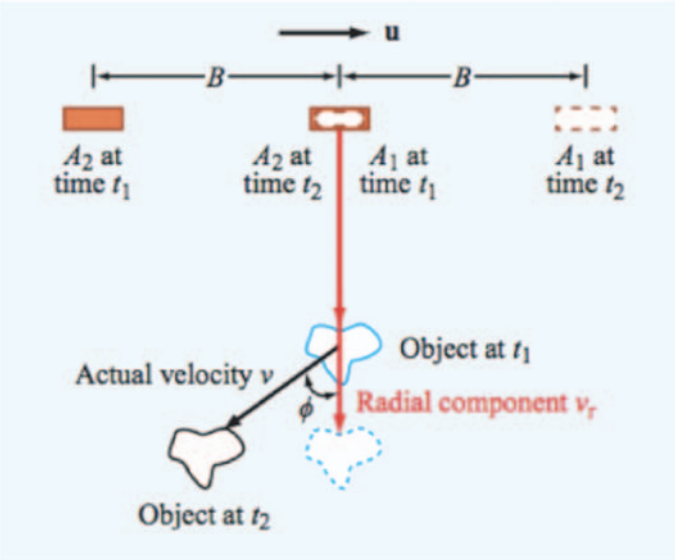

Figure 3. *Shows an object receding from the satellite during t_1 and t_2 taken by A_1 and A_2 respectively. The useful information is the radial velocity, v_r that will provide how fast the object is moving relative to the satellite. Figure from Ulaby and Long, 2014.*

The above equation (1.6) is a great method of measuring the velocity of an object that tends to be constantly moving, such as ocean currents (Ulaby and Long, 2014).

Surface deformation studies tend to use the exactly same concepts and techniques to measure phase differences. The only modification would be, conventionally, that satellites are used instead of aeroplanes, and the time difference between two non-spatial SAR images could be days or weeks contrasted to the milliseconds on a fixed aeroplane. This allows for the study and measurement of surface deformation that takes place over a considerable period of time. Such examples could include: glacial travel, volcanic deflation, and tectonic plate movement (Figure 4).

However, studies can also be conducted on areas that experienced sudden deformation, such as in earthquakes, tsunamis, and landslides. Using ERS-1 SAR images over

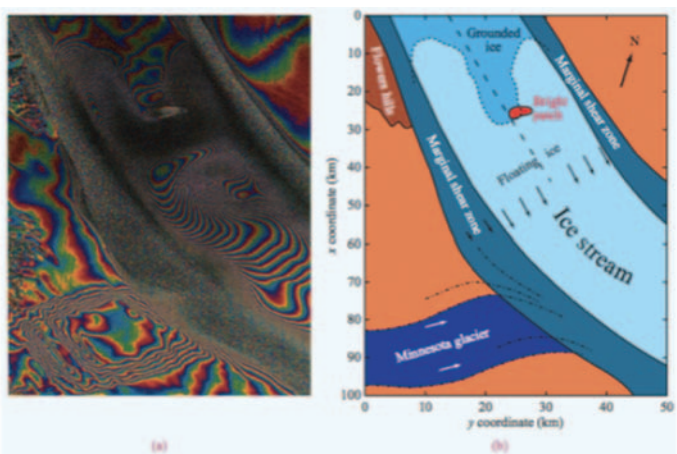

Figure 4. *InSAR diagram of the Rutford ice stream in Antarctica. The map on the left is essentially the fringe pattern that represents the surface deformation due to flowing ice. The closer the fringes are to each other the more deformation has occurred. To produce this diagram, the images were taken 6 days apart with the ERS-1 Satellite. Figure from Ulaby and Long, 2014.*

Antartica, Goldstein et al. (1988) demonstrated that the flow velocity of an ice stream could be measured with a precision of about $3 \times 10^{-8} \frac{m}{s}$ (Goldstein, 1993). As demonstrated in Eq. (1.6), the ratio $B/_u$ represents the time delay Δt between the two SAR images. Plugging these numbers into the equation gives us:

$$\pm v_r = \frac{\lambda}{4\pi \, sin\theta \, \Delta t} \phi_{int} \quad (1.7)$$

If two observations are 15 days apart and within the X-band range; $\theta = 45^{\circ}$ $\phi_{int} = 0.05$ radians; accuracy of satellite. Eq. (1.7) leads to:

$$v_r = \frac{0.03}{4\pi \cdot 15 \, days} \cdot 0.05$$

$$v_r = \frac{0.03}{4\pi \cdot 0.707 \cdot 15 \, days} \cdot 0.05$$

$$v_r = 1.1 \times 10^{-5} \frac{m}{day} = 0.41 \frac{cm}{year}$$

The measurement is comparable to the velocity of tectonic motion. This data shows that InSAR has the ability to measure surface deformation even for processes that are extremely slow. This same idea can be applied to tectonic episodes; the majority of tectonic movement isn't as fluid as that of glacial flow, but occurs in sudden incidents we can use Eq. (1.7) to be able to measure directly the topographic change in elevation. Consider an earthquake that strikes without notice. As shown in Figure 5, using the two different phase delay information, it is possible to straightforwardly quantify the difference in elevation due to the earthquake. Breaking apart Eq. (1.4):

$$\phi(t_1) = -\frac{4\pi}{\lambda} R_1 + \phi_{s1} \quad (1.8)$$

$$\phi(t_2) = -\frac{4\pi}{\lambda}(R_1 - \Delta R) + \phi_{s2} \quad (1.9)$$

Eq. (1.8) and (1.9) corresponds to image 1 and 2 from Figure 5 respectively. Assuming the backscatter of both SAR images are equivalent $\phi_{s1} = \phi_{s2}$, it can be shown that directly measuring the interferometry phase can result in a direct quantity that parallels the topographic elevation change. From Eq. (1.4), (1.8), and (1.9) it is revealed that the measurement can be comprised by two factors (1) changes in the surface scatters causing $\phi_{s1} \neq \phi_{s2}$, and (2) deviation in the satellite orbit between the two observations permitting topographic responses to be leaked into the data (Ulaby and Long, 2014). A technique known as stacking is most commonly used on satellite interferometry to remove data that could potentially pose a threat to quality data. This idea is simple enough that instead of a two-pass track, the SAR detector forces an nth –pass to obtain more SAR images that are essentially 'stacked' upon one another. This method is useful in the sense that is reduces statistical errors, but it only yields a single average deformation measurement (Ulaby and Long, 2014). It is almost impossible to be able to retrieve time history measurements from a multi stacked (added) interferometry diagram; this is also known as time-series InSAR applications.

Unwrapping phase

The methods used to recover phase delays in each individual pixel are important, because they allow for the extraction of phase difference. The biggest problem that faces scientists, who

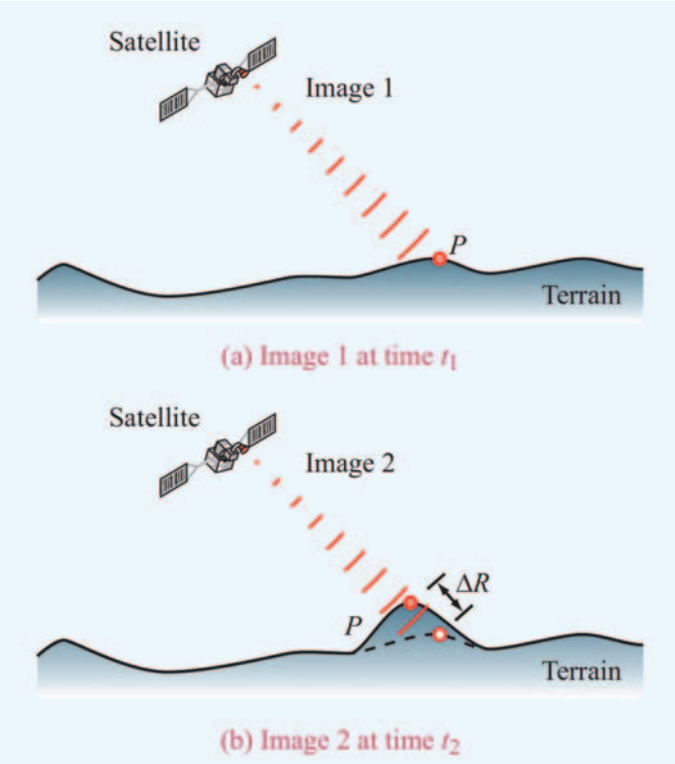

Figure 5. *Image 1 shows the first SAR image of a satellite with its own unique phase delay + phase backscatter. Image 2 is taken after a sudden tectonic event happens that brings the ground closer to the SAR detector. This results in a unique phase delay, assuming, for simplicity, that both backscatter responses are identical. Figure from Ulaby and Long, 2014.*

are interested in a particular value that corresponds to an elevation change, comes back to the previous topic of Modulo-2π. The data is very limited if the information just displays a phase difference. This is because the information shows an interferometric phase has taken place, but not how many integer wavelengths it took to obtain said phase. Therefore, it is almost impossible to obtain any practical elevation difference unless a process known as unwrapping is used, which has both great advantages and disadvantages.

Interferometry records data in complex format – Euler's Identity,

$$e^{j\theta} = cos\theta + jsin\theta \quad (1.10)$$

It cycles between π and π; due to the nature of electromagnetic waves. The signal that is true, and resembles the true amount of wavelengths to target, is hidden or wrapped to the values that are the remainder after dividing the full value by 2π. Phase unwrapping is the process of reversing and attempting to reconstruct the true, unwrapped signal from the wrapped interferogram (Nee, 2012). To obtain such results many techniques and algorithms have been invented over the years, and attempts are constantly being made to make the process more precise and accurate. That development process is, however, beyond the scope of this review. Snaphu is the most popular unwrapping algorithm that has been incorporated in much of the free-source InSAR processing packages such as GMTSAR and ROI PAC (Chen and Zebker, 2003).

Academic applications

InSAR has been in the academic world since its inception, and many papers have been written about its applications. The most

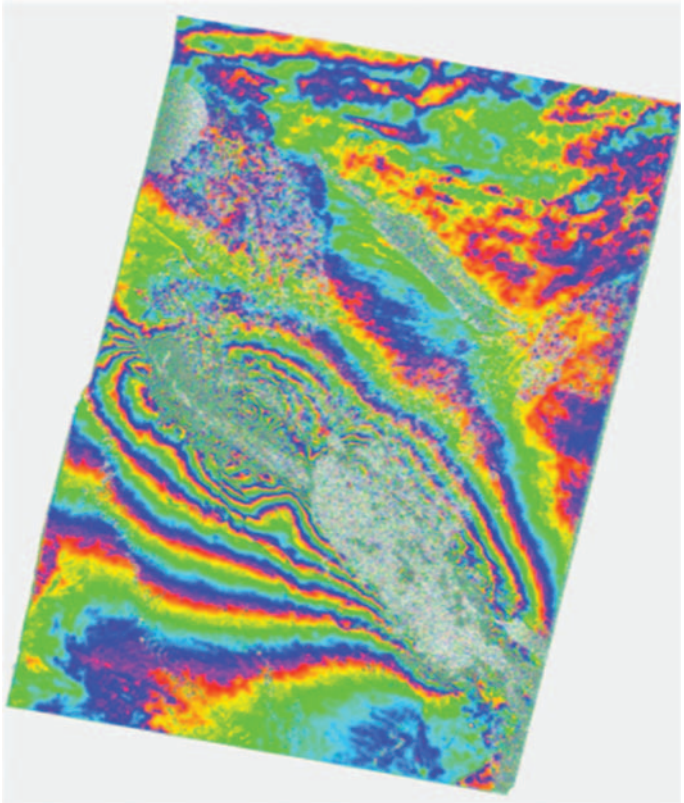

Figure 6. *An InSAR image of Baja California processed using GMTSAR. The image shows a close fringe pattern towards its centre, which indicates the extent of surface deformation resulting from the earthquake. Figure from GMTSAR, 2010.*

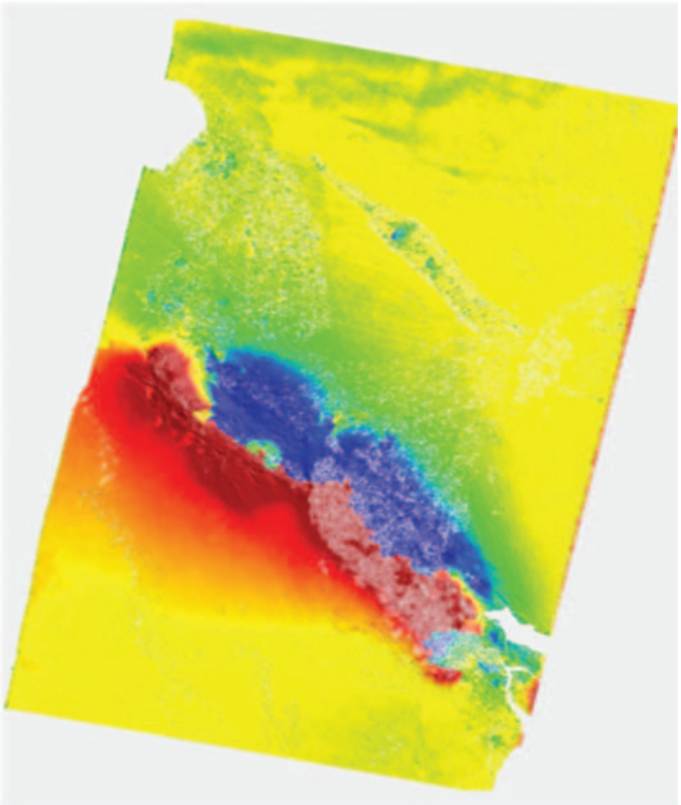

Figure 7. *An unwrapped image over Baja California, which is much easier to interpret than the complex interferogram shown in Figure 6. The red colour indicates the area has moved closer to the SAR sensor. In contrast, the blue colour indicates areas that have moved farther away. Figure from GMTSAR, 2010.*

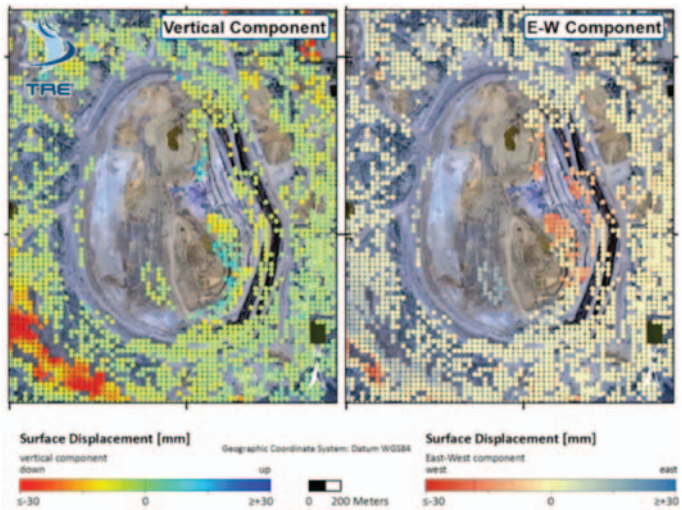

Figure 8. *Images showing an open-pit diamond mine in South Africa. The image on the left shows points that correlate to vertical displacement on the pit-slopes. As can be seen, the area on the bottom left of the image is highly active in terms of vertical displacement. The image on the right shows the same open-pit mine, but with points correlating to shear displacement. This data demonstrates the practical significance of InSAR. Figure from Colombo and MacDonald, 2015.*

notable scientists to use InSAR are: Zebker, Chen, Hensley, Rosen, and Ferretti. An important case study, conducted by Rosen in 1994, demonstrated the measurement of surface deformation due to volcanic inflation in Hawaii. The results were compared to GPS data to verify that InSAR has similar accuracy potential. Many disciplines of InSAR exist, but the end goal of any discipline is to compare two or more SAR image phase delays. The only prominent difference lies in the different techniques used to account for the various factors that can affect what the target of interest would be. In the Hawaiian case, a process known as Differential Interferometry (DinSAR) was used to measure the centimetre scale deformation of an active caldera over a period of six months (Rosen et al., 1996). Differential InSAR is the most common process whereby a SAR image, known as a master, is taken at a certain time interval. After a period of time has passed, another SAR image, a slave, is taken of the same area. In theory, it is easy to calculate the interferometry between two SAR images, assuming that no spatial distance has taken place. However, in the real world, a satellite does not exactly retrace its steps perfectly, and because of this even the slightest shift from the original position can cause the data to be ruined by the addition of topographic phase response. This problem can be resolved by introducing a DEM (Digital Elevation Model) of the area. The DEM allows any response due to topography to be 'zeroed' out, but it is only as accurate to the level of resolution provided by the DEM.

The study of volcanic inflation/deflation is common, as is the study of sudden surface deformation such as that created by earthquakes. Using InSAR a group of scientists followed a swarm of earthquakes that occurred in western United States of America in the Columbian River Flood Basalts (Wicks et al., 2011). Figure 6 shows an interferometry image of an area over Baja California taken by ENVISAT. The image shows a close fringe pattern towards its centre, which indicates the extent of surface deformation resulting from the earthquake. It can be tough when interpreting the data to know how the elevation has changed and by how much, and this is where unwrapping becomes useful. Figure 7 shows the same image, but this time it has been unwrapped using Snaphu, allowing for easier interpretation. Unwrapping is only as accurate as algorithms that govern it, but is accurate enough for most practical purposes.

Industry applications

InSAR has yet to make a real impact in industry. One of the world's leading researchers and engineers, and the EAGE Visiting Lecturer in Australia in 2015, Alessandro Ferretti, has repeatedly demonstrated just how useful InSAR could be from a business standpoint. According to Ferretti, InSAR data can be used for fault characterization and calibration of geo-mechanical models in the oil and gas sector, for monitoring landslides, volcanoes, faults, and areas prone to sinkholes and subsidence, for understanding terrain compaction phenomena induced by tunnelling works, and even for monitoring the stability of individual buildings (Ferretti et al., 2015).

In Australia the mining industry could use InSAR to monitor the stability of mine sites. In the past it was almost impossible to remotely monitor mine sites due to the long revisiting time frame of available satellites. However, that is not a problem with modern satellites[1] (Colombo and MacDonald, 2015). Colombo and MacDonald studied an open-pit diamond mine in South Africa. The stability of the pit walls was of particular concern as it was feared a landslide would damage valuable assets. As shown in Figure 8, points on the open-pit showed vertical and shear displacements. The data identified areas at risk of failure and highlights the value of InSAR in mine site assessment and monitoring; potentially saving assets and the lives of mine workers.

Processing

Many commercial products exist that support InSAR data processing. However, there are also a number of open-source packages that are available online. The most common and powerful suites obtainable are: GMTSAR, ROI PAC, and NEST-Snap (Alaska Satellite Facility, 1991). The first named is a command-line utility that is built off the famous GMT (Generic Mapping Tools) that was created by Paul Wessel and others at the University of Hawaii (Wessel, 2013). Many routes can be taken to process InSAR data. GMTSAR processes and procedures are only given as an example.

GMTSAR processing

GMTSAR[2] takes raw data from the major satellites[3] that provide high-quality SAR imagery and processes the data in six steps: (1) Assuming data is downloaded in raw format, known as Level 0 data (L0), from their respective platforms GMTSAR first processes the raw data to a format that is compatible to the inner workings of the platform. (2) The second stage is governed by a series of GMT shell scripts and compiled C files that align and focus the satellite data. This is needed in order for the two, or more, SAR images to be precisely aligned with one another so each master cell's phase delay can be compared with the slave(s). After alignment and focusing has been completed the data set has evolved to Level 1 data (L1). GMTSAR then produces a DEM of the area of interest to compare with L1 data. (3) The DEM, which is a gridded file, is used to eliminate any

[1] COSMO-SkyMed Satellite: 8-day revisit period for example.
[2] http://topex.ucsd.edu/gmtsar/.
[3] ALOS-1, ALOS-2, Envisat, ERS, COSMOS-Sky, Radarsat, Sentinel-1A, and TerraSAR-X.

topographic phase response from the master file, allowing for (4) an interferogram to be created using any filters that may have been provided; this results in an image as shown in Figure 6. Depending on whether unwrapping is required, (5) GMTSAR will use its built-in unwrapper, Snaphu, to produce the unwrapped version of the interferogram, as in Figure 7. Finally (6), GMTSAR finishes up by converting all calculated data into readable formats. This includes image and Google Earth[4] files that can easily be reproduced and shared. GMTSAR and other freely available processing software are powerful resources for potential users of InSAR. Enjoy!

Mathematical proofs

$$1.1\ S(t) = Acos[2\pi f_o(t-\tau)]$$

$$\Rightarrow S(t) = Acos[2\pi f_o\left(t - \frac{2x}{c}\right)]$$

$$\Rightarrow S(t) = Acos\left[2\pi f_o t - \frac{4\pi x}{c} f_o\right]$$

$$\Rightarrow S(t) = Acos\left[2\pi f_o t - \frac{4\pi x}{c} \cdot \frac{c}{\lambda}\right]$$

$$\Rightarrow S(t) = Acos\left[2\pi f_o t - \frac{4\pi}{\lambda} x\right]$$

$$1.2\ S(t) = Acos[2\pi f_o t - \phi]$$

$$1.3\ R_2 = R_1 \pm \frac{B}{u} v_r\ sin\theta$$

$$1.4\ \phi_{int} = -\frac{4\pi}{\lambda}(R_1 - R_2)$$

$$\Rightarrow \phi_{int} = -\frac{4\pi}{\lambda}\left(R_1 - R_1 \mp \frac{B}{u} v_r sin\theta\right)$$

$$\Rightarrow \phi_{int} = -\frac{4\pi}{\lambda}\left(\mp \frac{B}{u} v_r\ sin\theta\right)$$

$$1.5\ \phi_{int} = \pm \frac{4\pi}{\lambda u} B v_r\ sin\theta$$

$$1.6\ \pm v_r = \frac{\lambda u}{4\pi B\ sin\theta}\ \phi_{int}$$

$$\Rightarrow \pm v_r = \frac{\lambda}{4\pi\ sin\theta} \cdot \frac{u}{B}\ \phi_{int}$$

$$\Rightarrow \pm v_r = \frac{\lambda}{4\pi\ sin\theta} \cdot \frac{1}{\Delta t}\ \phi_{int}$$

$$1.7\ \pm v_r = \frac{\lambda}{4\pi\ sin\theta\ \Delta t}\ \phi_{int}$$

$$1.8\ \phi(t_1) = -\frac{4\pi}{\lambda} R_1 + \phi_{s1}$$

$$1.9\ \phi(t_2) = -\frac{4\pi}{\lambda}(R_1 - \Delta R) + \phi_{s2}$$

$$1.10\ e^{j\theta} = cos\theta + jsin\theta$$

References

Alaska Satellite Facility, 1991, *Alaska Satellite Facility making remote sensing data accessible since 1991.* https://www.asf.alaska.edu/data-tools/other-software-tools/ (accessed 2016).

Canadian Space Agency, 2014, *RADARSAT-1.* 21 March. http://www.asc-csa.gc.ca/eng/satellites/radarsat1/ (accessed 2016).

Canadian Space Agency, 2015, *Satellite characteristics.* 7 October. http://www.asc-csa.gc.ca/eng/satellites/radarsat/radarsat-tableau.asp (accessed 2016).

[4] https://earth.google.com.

Chen, C. W., and Zebker, A. H., 2003, *SNAPHU: statistical-cost, network-flow algorithm for phase unwrapping.* http://web.stanford.edu/group/radar/softwareandlinks/sw/snaphu/ (accessed 19 April 2016).

Colombo, D., and MacDonald, B. 2015, *Using Advanced InSAR Techniques as a Remote Tool for Mine Site Monitoring.* Slope Stability, The Southern African Institute of Mining and Metallurgy, Milan.

Engineering and Technology History, 2015, *Synthetic Aperature Radar.* http://ethw.org/Synthetic_Aperture_Radar (accessed 29 March 2016).

Ferretti, A., 2013, *Satellite inSAR Data Reservoir Monitoring from Space*. EAGE.

Ferretti, A., Fumagalli, A., Colombo, D., Novali, F., and Rucci, A. 2015, *InSAR data for monitoring land subsidence: time to think big.* Report, Milano: Open Access PIAHS.

GMTSAR, 2010, *Software, Documentation, Orbits, and Sample Data Downloads.* http://topex.ucsd.edu/gmtsar/tar/ENVI_Baja_EQ.tar.gz (accessed 19 April 2016).

Goldstein, R. M., 1993, Satellite radar interferometry for monitoring ice sheet motion: application to an Antarctic ice stream: *Science*, **262**(5139), 1525–1530. doi:10.1126/science.262.5139.1525

Goldstein, R. M., Zebker, H. A., and Werner, C. L., 1988, Satellite radar interferometry: two-dimensional phase unwrapping: *Radio Science*, **23**(4), 713–720. doi:10.1029/RS023i004p00713

GSI, 2004, *History of inSAR.* http://vldb.gsi.go.jp/sokuchi/sar/mechanism/history01-e.html (accessed 2016).

Hensley, S., and Rosen, P. A. S., 2001, Synthetic aperture radar interferometry: *IEEE* 88, no. 3 (November).

Lasswell, S. W., 2005, History of SAR at Lockheed Martin (previously Goodyear Aerospace): *Proceedings of the Society for Photo-Instrumentation Engineers*, **5788**, 1–12. doi:10.1117/12.603927

Nee, P., 2012, Phase unwrapping and inversion resolution of interferometric synthetic aperture radar geodesy. MSc Thesis, Faculty of Graduate School, Cornell University.

Rosen, P. A., Hensley, S., Zebker, H. A., and Webb., F. H., 1996, 'Surface deformation and coherence measurements of Kilauea Volcano, Hawaii, from SIR-C radar interferometer.' *Journal of Geophysical Research,* **101**, 23109–23125.

Ulaby, F. T., and Long, D. G., 2014, *Microwave Radar and Radiometric Remote Sensing.* (Ed. A. Arbor.) Michigan: The University of Michigan Press.

UNSW, 2004, *A Brief History – inSAR.* http://www.sage.unsw.edu.au/currentstudents/ug/projects/Walsh/History.htm (accessed 2016).

Wessel, P. 2013, *GMT.* http://gmt.soest.hawaii.edu/ (accessed 2016).

Wicks, C., Thelen, W., Weaver, C., Gomberg, J., and Rohay, A., 2011, InSAR observations of aseismic slip associated with an earthquake swarm in the Columbia River flood basalts: *Journal of Geophysical Research*, **116**(no. B12304). doi:10.1029/2011JB008433

Duan Uys is currently a Masters student at Macquarie University in Sydney, Australia. His research is focused on the application of InSAR to monitoring slope stability, particularly in areas where slope failure could result in loss of life. He believes that InSAR is currently underrated as a monitoring tool by the scientific community and is hoping that his work will change perceptions in that regard.